Ion energetics in collisionless sheaths of rf process plasmas

Cite as: Physics of Fluids B: Plasma Physics **4**, 2362 (1992); https://doi.org/10.1063/1.860206
Submitted: 06 November 1991 . Accepted: 24 February 1992 . Published Online: 04 June 1998

S. Hamaguchi, R. T. Farouki, and M. Dalvie

Ion energetics in collisionless sheaths of rf process plasmas*

S. Hamaguchi,† R. T. Farouki, and M. Dalvie
IBM Thomas J. Watson Research Center, Yorktown Heights, New York 10598

(Received 6 November 1991; accepted 24 February 1992)

Ion energy distribution functions in collisionless radio-frequency (rf) sheaths are discussed from the viewpoint of kinetic theory. Effects of rf fields on ion density and velocity profiles in plasma sheaths are also derived, based on ion fluid equations. It is shown that the ponderomotive force due to rf modulation of the magnitude of the sheath electric field exerts a retarding effect on the ion motion that counteracts the dc-bias field when the ratio of the ion transit frequency ω_{tr} to rf modulation frequency ω is small but finite. Consequently, the time-averaged ion density is higher and the time-averaged ion fluid velocity is lower in rf sheaths by the order of $(\omega_{tr}/\omega)^2$ than those in corresponding dc sheaths. The influence of an oscillating plasma/sheath boundary on the ion energetics is also considered. Under suitable conditions, this induces rapid "quasiperiodic" variations in the ion energy distribution as the rf ω is increased.

I. INTRODUCTION

Low-temperature, partially ionized plasmas are widely used in integrated-circuit fabrication processes, such as sputtering, etching, and chemical vapor deposition. At low pressures, such plasmas provide a directed flux of energetic ions impinging on semiconductor wafers attached to the electrodes, resulting in the "anisotropic" evolution of microfeature profiles. Since recent technological advances require increasingly fine structure to be produced with high accuracy, the control of process plasmas has become an important research topic.

Radio-frequency (rf) is commonly used as a means of generating, sustaining, and controlling process plasmas. Unlike dc discharges, rf discharges are capable of generating high dc "self-bias" sheath voltages, even for electrodes covered by insulating materials. Radio frequency voltages are also often applied to substrates that are exposed to high-density plasmas generated by other means, such as electron cyclotron resonance (ECR), providing control over the dc-bias voltage and the energy distribution of the incident-ion flux. Radio frequencies ω used are typically in the range 1–100 MHz. In the limit $\omega \to \infty$, most plasmas characteristics averaged over an rf cycle are similar to those of corresponding dc discharges, since the massive ions then experience only time-averaged electric fields.

The effects of ion inertia may be quantified by comparing the rf with the ion transit frequency $\omega_{tr} \simeq (qV/md^2)^{1/2}$ across the sheath. Here V and d represent a typical rf-sheath voltage and thickness, while q and m denote the ion charge and mass. For a helium discharge with $V=100$ V and $d=1$ mm, we have $\omega_{tr}/2\pi=7.8$ MHz. In such a case, where the rf is comparable to ω_{tr}, the ion trajectories across the sheath will be strongly influenced by the rf modulation of the sheath field.

In this paper we review recent results on ion energetics in collisionless rf sheaths;[1,2] related work on dc sheaths may be found in Refs. 3 and 4. The goal of these studies is to develop a deeper understanding of the factors influencing the incident-ion energy distributions in rf discharges. The precise form of these distributions is of practical importance in optimizing various plasma-assisted etching and deposition processes used in VLSI fabrication. The results presented below may be compared with typical experimental measurements[5,6] and numerical simulations.[7,8]

II. ION ENERGY DISTRIBUTIONS IN rf SHEATHS

Reviewing our recent work,[1] we now discuss incident-ion energy distributions in low-pressure rf discharges, in which a prescribed time-periodic electric field potential is given as $\Phi(z,t)=\Phi_0(z)+\Phi_1(z)\cos\omega t$. This may be regarded as the lowest-order approximation in the Fourier expansion of a general time-periodic field. An oscillatory motion of the relatively sharp presheath/sheath boundary may not be well described by this sinusoidally approximated field; see Sec. III for an analysis of ion distributions in rf sheaths with a sharp oscillatory boundary.

The ions are assumed to enter the sheath at position $z=0$ with the sound speed $v_B=(k_B T_e/m)^{1/2}$, where k_B is the Boltzmann constant and T_e is the electron temperature of the bulk plasma (this is the Bohm sheath criterion; see Ref. 9), and with zero ion temperature, $v_\perp=0$. Since only a collisionless rf sheath is considered, the ion distribution is a time-periodic function of space z and the velocity component v_z, governed by the following Vlasov equation:

$$\frac{\partial f}{\partial t}+v_z\frac{\partial}{\partial z}-\frac{q}{m}\frac{\partial\Phi(z,t)}{\partial z}\frac{\partial f}{\partial v_z}=0. \tag{1}$$

Here the distribution function $f(t,z,v_z)$ may be considered to have already been integrated over $v_\perp$. The boundary condition for f is then given by $f(t,z=0,v_z)=n_I\delta(v_z-v_B)$, where n_I denotes the ion density at $z=0$.

The characteristic equation for the Vlasov Eq. (1) is given by

*Paper 9I6, Bull. Am. Phys. Soc. **36**, 2483 (1991).
†Invited speaker.

 0899-8213/92/072362-06$04.00

$$\frac{dv_z}{dt}=\frac{q}{m}[E_0(z)+E_1(z)\cos\omega t], \tag{2}$$

where $E_0(z)=-d\Phi_0/dz$ and $E_1(z)=-d\Phi_1/dz$. Equation (2) is Newton's law for the ion trajectory. The initial conditions for Eq. (2) are that the ion is injected into the sheath with fixed velocity v_B at position $z=0$ and at any given time $t=t_I$.

In the high-frequency regime, where the inequality

$$\varepsilon\equiv\frac{1}{\omega}\left(\frac{qE_0(d)}{md}\right)^{1/2}\ll 1$$

holds, we have solved Eq. (2) using a two-time-scale asymptotic expansion in Ref. 1. The resulting expression for the velocity v_z of the ion when it reaches the cathode ($z=d$) at time t is given by

$$v_z=[v_B^2-2q\Phi_0(d)/m]^{1/2}+[qE_1(d)/m\omega]\sin\omega t. \tag{3}$$

It should be noted that $\varepsilon^2=(\omega_{tr}/\omega)^2$, where $\omega_{tr}\equiv[qE_0(d)/md]^{1/2}$ denotes a typical ion transit frequency across the sheath.

Writing the ion velocity at the cathode ($z=d$) due to the dc-bias (i.e., time-averaged) field $\Phi_0(z)$ as $v_{max}\equiv\sqrt{v_B^2-2q\Phi_0(d)/m}$, and defining $\eta\equiv v_z^2/v_{max}^2$, we compute the energy distribution Γ_{EN} of the ion flux at position z as $\Gamma_{EN}\,d\eta=v_z f(t,d,v_z)dv_z$, i.e., $\Gamma_{EN}=\frac{1}{2}v_{max}^2 f(t,d,v_z)$. Then the experimentally observed ion energy flux distribution is the time average of Γ_{EN}:

$$\overline{\Gamma_{EN}}=\frac{\omega}{2\pi}\int_0^{2\pi/\omega}\Gamma_{EN}\,dt.$$

The solution (3) to the Vlasov Eq. (1) is used to calculate the time-averaged energy distribution $\overline{\Gamma_{EN}}$ in the high-frequency regime ($\omega\gg\omega_{tr}$), and we obtain[1]

$$\overline{\Gamma_{EN}}(\eta)=n_I v_B/2\pi\sqrt{(\nu_+-\sqrt{\eta})(\sqrt{\eta}-\nu_-)}, \tag{4}$$

where $\nu_\pm=1\pm qE_1(d)/m\omega v_{max}^2$.

We now compare the analytical expression, Eq. (4), to numerical simulations for a given "idealized" electric field profile $E_0(z)=E_1(z)=-d\Phi_0/dz$. Here Φ_0 is the collisionless dc sheath potential subject to the boundary conditions $\Phi_0(0)=0$ and $d\Phi_0(0)/dz=-E_I$.[1,3,4] The electric field profile used in the following calculations is the same as that used in Ref. 1.

Figures 1(a) and 1(b) show the analytical expression, Eq. (4), and the direct integration of Eq. (2) with uniformly distributed random initial phase $\phi=\omega t_I$, obtained from a simulation program similar to the Monte Carlo code described in Refs. 1 and 3, for two different values of ε: $\varepsilon=0.24$ for (a), and $\varepsilon=0.16$ for (b). A good agreement between the analytic formula and the simulation results is evident in Fig. 1. It should be noted, however, that higher-order effects that have been dropped in the asymptotic analysis [i.e., in deriving Eq. (3)] are also seen in the numerical simulations, as an asymmetry of the energy distribution profiles about $\eta=1$. The analytic expression, Eq. (4), becomes symmetric around $\eta=1$ in the $\varepsilon\to\infty$ limit. Any asymmetry suggested by the analytical expression, Eq. (4), which arises due to finite values of ε, should be considered as a higher-order effect. Therefore, discrepancies in the slight asymmetry of the analytical and numerical energy distributions profiles are expected to be visible in Fig. 1.

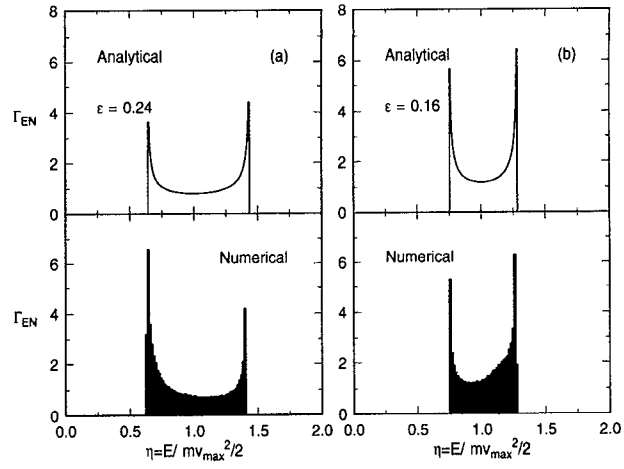

FIG. 1. The energy distributions of the ion flux at the cathode ($z=d$) obtained from the analytical expression Eq. (4) and numerical simulations based on Eq. (2). The parameters used here are $v_B/d\omega=0.02$, and $\varepsilon=0.24$ for (a) and $\varepsilon=0.16$ for (b), which correspond to an argon discharge with the dc-bias sheath potential $-\Phi_0(d)=35$ V, $d=0.83$ mm, $\omega/2\pi=8.7$ MHz for (a), and $\omega/2\pi=13.0$ MHz for (b). In the analytic expressions, the singularities are truncated by plotting $\overline{\Gamma_{EN}}(\eta)$ for $\nu_-^2-\delta\eta\leqslant\eta\leqslant\nu_-^2$ with $\delta\eta/[-2\Phi_0(d)]=0.007$. In each case, $\overline{\Gamma_{EN}}$ is normalized so as to enclose unit area.

The energy distribution $\overline{\Gamma_{EN}}$ given in Eq. (4) has singularities as $\eta=v_+^2$ and v_-^2, defining the limits of energy spread. The width of the energy spread $\Delta\mathscr{E}=\frac{1}{2}mv_{max}^2\Delta\eta$, where $\Delta\eta=v_+^2-v_-^2$, is thus given by

$$\Delta\mathscr{E}=2v_{max}qE_1(d)/\omega. \tag{5}$$

Figure 2 shows the width of the energy spread $\Delta\mathscr{E}$ as a function of ε (i.e., the inverse of the radio frequency) under the same conditions as those of Fig. 1. It is seen that the formula (5) gives a reasonable estimate of the energy

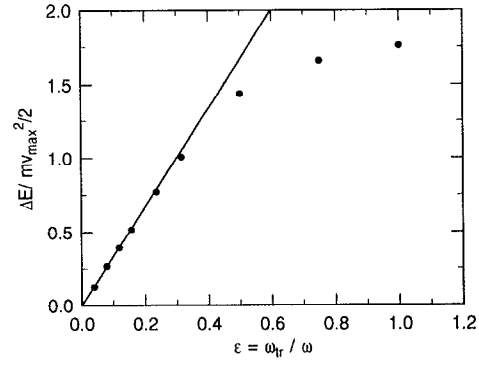

FIG. 2. The width of the energy spread $\Delta\eta=\Delta\mathscr{E}/\frac{1}{2}mv_{max}^2$ as function of $\varepsilon=\omega_{tr}/\omega$. The solid line is from the formula given in Eq. (5), while the dots represent numerical simulations. The numerical parameters used in these calculations are the same as those in Fig. 1.

spread when $\varepsilon \lesssim 0.4$. Since the final velocity $v_{\max}$ may be approximated by $v_{\max} \simeq [-2q\Phi_0(d)/m]^{1/2}$, we obtain the scaling $\Delta\mathscr{E} \propto m^{-1/2}$ from Eq. (5), as discussed in Refs. 5 and 10. [The expression $\Delta\mathscr{E} = (-8q\Phi_1/3\omega d)(-2q\Phi_0/m)^{-1/2}$ was derived in Ref. 10, based on the assumption that $\Phi_0 \gg \Phi_1 \propto (z/d)^{4/3}$. This expression for $\Delta\mathscr{E}$ is easily derived from our general formula, Eq. (5), under the conditions that $v_B^2 \ll -2q\Phi_0(d)/m$ and $\Phi_1(z) \propto (z/d)^{4/3}$.] The formula (5) also explains the experimental observation of Coburn and Kay (Fig. 12 in Ref. 5) that the scaling $\Delta\mathscr{E} \propto m^{-1/2}$ fails as $m^{-1/2} \to 0$: since $v_{\max} \to v_B$ in this limit, it is clear from Eq. (5) that $\Delta\mathscr{E}$ becomes independent of the ion mass m.

III. ION ENERGETICS IN OSCILLATING-BOUNDARY SHEATHS

The self-consistent, time-periodic structure of a rf sheath can be quite complex, the electric field profile varying continuously in magnitude, extent, and shape during the rf cycle. In the model discussed above, incident-ion energy distributions were derived, in the high-frequency regime, for sheaths of fixed width and a field profile whose magnitude is modulated sinusoidally with time. In real rf sheaths, however, the high mobility of the electron gas can be expected to result in a relatively sharp plasma/sheath boundary oscillating in sympathy with the rf excitation. To assess the influence of such an oscillatory boundary on the incident-ion energy distribution, we have analyzed in detail a simple model[2] in which the sheath field is spatially constant, but the sheath width is sinusoidally modulated in time. In this section we briefly review the salient features of this model.

We assume a low-pressure rf discharge, with collisionless ion transport across the sheath. The ion equation of motion is

$$\frac{d^2z}{dt^2} = \frac{qV_s}{md} H[z + d\cos(\omega t + \phi)], \tag{6}$$

where H is the Heaviside step function [i.e., $H(x)=1$ if $x \geqslant 0$ and $H(x)=0$ otherwise], with initial conditions $z(0) = -d$ and $dz/dt|_{t=0} = v(0) = v_B$. Here d and V_s are the mean sheath thickness and potential drop. The quantity $z_s(t) = -d\cos(\omega t + \phi)$ gives the location of the plasma/sheath boundary, which oscillates between $-d$ and $+d$. The phase ϕ of this oscillation upon introduction of any ion is assumed to be random between $-\pi$ and $+\pi$, i.e., the (monoenergetic) ion flux incident on the plane $z=-d$ is constant in time. The cathode is at $z=+d$.

The ion trajectories are governed by the dimensionless quantities $\alpha = qV_s/m\omega^2 d^2$, the *acceleration parameter*, and $\beta = v_B/\omega d$, the *initial velocity parameter*. These trajectories are characterized by alternating intervals of uniform acceleration and "coating" at constant velocity, whose number and relative duration are determined by the initial phase ϕ.

Introducing the dimensionless time, position, and velocity variables $\tau = \omega t$, $\xi = z/d$, and $\mu = v/\omega d$, the instances τ_k at which an ion introduced at phase ϕ crosses the boundary, and the corresponding locations ξ_k and velocities μ_k, are determined by the concatenated system of equations

$$f_k(\tau) = \xi_k + \mu_k(\tau - \tau_k) + (\alpha_k/2)(\tau - \tau_k)^2 + \cos(\tau + \phi) = 0 \tag{7}$$

for $k=0,1,\ldots$, which commences with $\tau_0 = 0$, $\xi_0 = -1$, $\mu_0 = \beta$, and $\alpha_0 = 0$. The value of $f_k(\tau)$ gives the difference between the position of the ion and the plasma/sheath boundary. The desired solution to Eq. (7) is defined as the *first* real root (if any) of $f_k(\tau)$ that is greater than τ_k. If such a root exists, it is assigned to τ_{k+1}. The coefficients ξ_{k+1} and μ_{k+1} of the succeeding equation $f_{k+1}(\tau) = 0$ are then determined by

$$\xi_{k+1} = \xi_k + \mu_k(\tau_{k+1} - \tau_k) + (\alpha_k/2)(\tau_{k+1} - \tau_k)^2, \tag{8}$$

$$\mu_{k+1} = \mu_k + \alpha_k(\tau_{k+1} - \tau_k), \tag{9}$$

while the quantity α_k is equal to α if k is odd (acceleration interval), and is 0 if k is even (coasting interval). The system (7) terminates on encountering an equation $f_n(\tau) = 0$ that has no real solution. The final velocity of the ion impinging on the cathode at $\xi = 1$ is then $\mu_{n+1} = \sqrt{2\alpha(1-\xi_n) + \mu_n^2}$.

An algorithmic method for solving the system of equations (7) at a suitably dense, uniformly spaced sequence of values of the initial phase ϕ is described in Ref. 2. Within the "transition regime," where the parameters α and β are neither very small nor greater than (or comparable to) unity, it is observed that the resulting families of ion trajectories always divide into groups, delimited by two "critical" values of the initial phase ϕ, that suffer N and $N+1$ immersions in the sheath field. The first critical phase depends only on β, and may be expressed analytically as

$$\phi_{\text{crit}}(\beta) = \sin^{-1}\beta - [(1 - \sqrt{1-\beta^2})/\beta]. \tag{10}$$

The significance of (10) is that, for an ion injected at this phase, the *first* encounter with the oscillating plasma/sheath boundary is only a "glancing" encounter (i.e., the ion does not cross the boundary). Note that $\phi_{\text{crit}}(\beta) \simeq \frac{1}{2}\beta + O(\beta^3)$ when β is small, i.e., $\phi_{\text{crit}}(\beta)$ does not vary much when $\beta \ll 1$.

The second critical phase, which we denote by $\varphi(\alpha,\beta)$, represents that phase at which the *last* encounter of an ion with the boundary is a glancing one. Although $\varphi(\alpha,\beta)$ admits no simple closed-form expression in terms of α and β, we observe empirically a relatively simple dependence on these parameters. Namely, reducing α and/or β (e.g., increasing ω with all other sheath variables held constant) always drives $\varphi(\alpha,\beta)$ to lower values. Thus, the second critical phase cycles continuously as the rf is systematically increased. Associated with each such cycle, the fraction of ions that suffer $N+1$ immersions in the field increases at the expense of those that suffer that N—until, as $\varphi(\alpha,\beta)$ passes through $\phi_{\text{crit}}(\beta)$, we enter a regime in which ion trajectories are divided into groups that suffer $N+1$ and $N+2$ acceleration intervals.

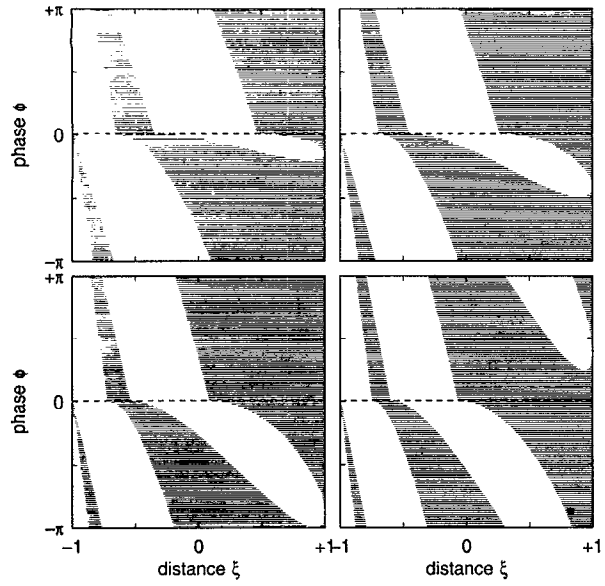

FIG. 3. Illustration of the "cycling" of the second critical phase $\varphi(\alpha,\beta)$ as the rf ω increases. The disposition of the "coasting" (blank) and "acceleration" (solid) intervals of ion trajectories with respect to the initial phase ϕ is shown in four cases, corresponding to $\sim 10\%$ increases in ω. The dashed line indicates the first critical phase, $\phi_{\rm crit}(\beta)$.

Qualitatively, this behavior persists indefinitely. In Fig. 3 we illustrate nearly a full cycle of $\varphi(\alpha,\beta)$ for the nominal physical parameters (assuming singly ionized O_2) $V_s \approx 270$ V, $d \approx 3$ mm, $v_B = \sqrt{k_B T_e/m}$ with $T_e \approx 10^5$ K, and ω increasing from 30 to ~ 40 MHz in three steps of roughly 10% each.

Corresponding to the cycling of $\varphi(\alpha,\beta)$, the ion energy spectrum exhibits rapid "quasiperiodic" variations, superposed on a systematic narrowing, as the frequency ω is increased. Since the electric field is spatially constant, the work done on an ion during each acceleration interval is proportional to the width $\xi_{k+1}-\xi_k$ of that interval. Thus, on arriving at the cathode, the final energy of an ion injected at phase ϕ (normalized to a maximum value of unity) is

$$\eta(\phi)=\frac{2\alpha[(1-\xi_n)+\cdots+(\xi_4-\xi_3)+(\xi_2-\xi_1)]+\beta^2}{4\alpha+\beta^2}, \tag{11}$$

where the locations $\xi_1,\xi_2,\ldots,\xi_n$ (and number n) of the boundary crossings depend on ϕ and on the sheath parameters α and β.

If the ion flux incident on the plane $\xi=-1$ from the plasma bulk is independent of phase ϕ in the rf cycle, the time-averaged energy distribution of the ion flux impinging on the cathode will be given simply by

$$\Gamma(\eta) \propto \sum_k \left|\frac{d\eta}{d\phi}\right|^{-1}_{\phi_k}, \tag{12}$$

where $\{\phi_k\}$ is the set of finitely many initial phases that yield a prescribed final ion energy η at the cathode. Note that $\Gamma(\eta)$ is singular at any energy η that is "stationary" with respect to the initial phase ϕ (i.e., $d\eta/d\phi=0$).

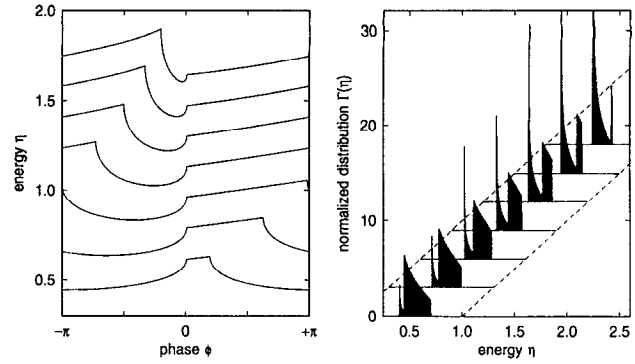

FIG. 4. Variation of the energy-phase relationship $\eta(\phi)$, and the normalized energy distribution $\Gamma(\eta)$ of the ion flux at the cathode, with frequency ω. For clarity, successive graphs of $\eta(\phi)$ are displaced by 0.2 vertical units; the scale on the energy axis holds for the lowermost graph, representing the highest frequency. Similarly, the $\Gamma(\eta)$ distributions at successively higher frequencies are displaced horizontally and vertically, the baseline for each plot representing the interval $0 \leqslant \eta \leqslant 1$. Successive cases represent $\sim 5\%$ increases in ω, from $(\alpha,\beta)=(0.1,0.06)$ at bottom left to $\sim(0.056,0.045)$ at top right.

Figure 4 illustrates the energy-phase relationships (11) and the corresponding energy distributions (12) for the system of Fig. 3, sampled at successive frequencies corresponding to $\sim 5\%$ increases in ω. For ions that suffer $N+1$ acceleration intervals—i.e., those introduced at phases between $\phi_{\rm crit}(\beta)$ and $\varphi(\alpha,\beta)$—$\eta(\phi)$ has a "parabolic" shape, contributing a spiked low-energy component to $\Gamma(\eta)$. For ions having just N acceleration intervals, $\eta(\phi)$ is nearly linear and contributes a broader high-energy component to $\Gamma(\eta)$.

As ω increases, the population of the low-energy component of $\Gamma(\eta)$ grows at the expense of the high-energy component, since the cycling of $\varphi(\alpha,\beta)$ causes an increasing fraction of the ions to experience $N+1$ rather than N immersions in the sheath field. This redistribution process commences anew, with the value of N incremented by unity, as $\varphi(\alpha,\beta)$ passes through $\phi_{\rm crit}(\beta)$ [at this juncture in the cycle, however, the behavior of $\Gamma(\eta)$ becomes somewhat more complicated].

The precise forms of the ion energy distributions in Fig. 4 are probably artifacts of the idealized sheath field model. The principal value of this study is intended to be in elucidating important physical effects that arise in the ion transport problem, and in providing a plausible, intuitive explanation of the observed double-peaked structures of ion energy distributions.

IV. FLUID EQUATIONS

In this section we consider ion fluid motion in rf sheaths, using again a sheath field of oscillating magnitude described by $E(z,t)=-\partial\Phi/\partial z=E_0(z)+E_1(z)\cos\omega t$. As before, the perpendicular flow velocity is assumed negligible ($v_\perp=0$). For low-pressure rf sheaths, the dynamics of the ion fluid is governed by the following mass-conservation and momentum-conservation equations:

$$\frac{\partial \hat{n}}{\partial \tau}+\varepsilon \frac{\partial}{\partial \zeta}(\hat{n}\hat{v})=0, \tag{13}$$

$$\frac{\partial \hat{v}}{\partial \tau}+\varepsilon \hat{v}\frac{\partial \hat{v}}{\partial \zeta}=-\varepsilon \frac{\partial \hat{\phi}}{\partial \zeta}, \tag{14}$$

with normalized variables $\tau=\omega t$, $\zeta=z/d$, $v_z=\varepsilon\, d\omega\, \hat{v}$, $\Phi=dE_0(d)\hat{\phi}$, $n=n_I\hat{n}$, and $\varepsilon^2=qE_0(d)/m\, d\omega^2$.

Here n and v_z denote the ion number density and the z-component ion flow velocity. The ion temperature is assumed to be small and the pressure term is dropped from the momentum conservation equation (14). The boundary conditions are that $\hat{n}(\zeta,\tau)$ and $\hat{v}(\zeta,\tau)$ are 2π periodic in τ, and satisfy $\hat{n}(0,\tau)=1$ and $\hat{v}(0,\tau)=u_B\equiv v_B/\varepsilon\, d\omega$ at the presheath/sheath boundary ($\zeta=0$). In the high-frequency regime (i.e., $\omega_{tr}\ll\omega$), $\varepsilon=\omega_{tr}/\omega$ becomes a small quantity and we solve Eqs. (13) and (14) using an asymptotic expansion.

In the infinite-frequency limit, the ions are expected to experience only the time-averaged electric field $E_0(z)$ due to their large inertia. Thus, in the limit $\omega\to\infty$, the lowest-order solution to Eqs. (13) and (14) must be derived from the following dc equations:

$$\frac{\partial}{\partial \zeta}(\hat{n}_0\hat{v}_0)=0, \tag{15}$$

$$\hat{v}_0\frac{\partial \hat{v}_0}{\partial \zeta}=-\frac{\partial \phi_0}{\partial \zeta}. \tag{16}$$

The solutions to Eqs. (15) and (16) are then given by $\hat{n}_0=u_B/\hat{v}_0$ and $\hat{v}_0=\sqrt{u_B^2-2\phi_0}$.

Although the dc-bias electric field E_0 and oscillating field E_1 are generally of the same order of magnitude, the perturbations to the density and velocity profiles due to the rf field $E_1(z)\cos\omega t$ are expected to be small in the high-frequency regime, $\varepsilon\ll 1$. Therefore, we write

$$\hat{n}=\hat{n}_0(\zeta)+\varepsilon\tilde{n}(\tau,\zeta),\quad \hat{v}=\hat{v}_0(\zeta)+\varepsilon\tilde{v}(\tau,\zeta),$$

$$\hat{\phi}=\phi_0(\zeta)+\phi_1(\zeta)\cos\tau,$$

where $\Phi_0=dE_0(d)\phi_0$ and $\Phi_1=dE_0(d)\phi_1$. The fluctuation components $\tilde{n}$ and $\tilde{v}$ then satisfy

$$\frac{\partial \tilde{n}}{\partial \tau}+\varepsilon\frac{\partial}{\partial \zeta}(\hat{n}_0\tilde{v}+\hat{v}_0\tilde{n}+\varepsilon\tilde{n}\tilde{v})=0, \tag{17}$$

$$\frac{\partial \tilde{v}}{\partial \tau}+\varepsilon\left(\hat{v}_0\frac{\partial \tilde{v}}{\partial \zeta}+\tilde{v}\frac{\partial \hat{v}_0}{\partial \zeta}+\varepsilon\tilde{v}\frac{\partial \tilde{v}}{\partial \zeta}\right)=-\frac{\partial \phi_1}{\partial \zeta}\cos\tau. \tag{18}$$

The boundary conditions at $\zeta=0$ are given by $\tilde{n}=\tilde{v}=0$. It is also assumed that the rf component of the electric field vanishes smoothly at the presheath/sheath boundary, i.e., $E_1(0)=dE_1(0)/d\zeta=0$. In order to solve Eqs. (17) and (18), we expand $\tilde{n}=\tilde{n}_1+\varepsilon\tilde{n}_2+\varepsilon^2\tilde{n}_3+\cdots$ and $\tilde{v}=\tilde{v}_1+\varepsilon\tilde{v}_2+\varepsilon^2\tilde{v}_3+\cdots$, assuming that $\tilde{n}$ and $\tilde{v}$ depend on ε analytically. Substituting these expressions into Eqs. (17) and (18), we obtain the lowest-order equations $\partial\tilde{n}_1/\partial\tau=0$ and $\partial\tilde{v}_1/\partial\tau=-\phi_1'\cos\tau$, where the prime denotes a derivative with respect to ζ (i.e., $'=\partial/\partial\zeta$). Integrating these equations yields $\tilde{n}_1=N_1(\zeta)$ and $\tilde{v}_1=\phi_1'\sin\tau+U_1(\zeta)$, where N_1 and U_1 are integration constants to be determined by higher-order equations. From the boundary conditions for $\tilde{n}_1$ and $\tilde{v}_1$, we have $N_1(0)=U_1(0)=0$. The second-order equations are given by

$$\frac{\partial \tilde{n}_2}{\partial \tau}+\frac{\partial}{\partial \zeta}(\hat{n}_0\tilde{v}_1+\hat{v}_0\tilde{n}_1)=0, \tag{19}$$

$$\frac{\partial \tilde{v}_2}{\partial \tau}+\hat{v}_0\frac{\partial \tilde{v}_1}{\partial \zeta}+\tilde{v}_1\frac{\partial \hat{v}_0}{\partial \zeta}=0. \tag{20}$$

Integrating these equations with respect to τ yields

$$\tilde{n}_2=-(\hat{n}_0\phi_1')'\cos\tau-(\hat{n}_0U_1+\hat{v}_0N_1)'\tau+N_2(\zeta), \tag{21}$$

$$\tilde{v}_2=-(\hat{v}_0\phi_1')'\cos\tau-(\hat{v}_0U_1)'\tau+U_2(\zeta). \tag{22}$$

The unbounded terms in time on the right-hand sides of Eqs. (21) and (22), which are called secular terms, must vanish due to the assumed boundedness of the terms $\tilde{n}_2$ and $\tilde{v}_2$ in time: $(\hat{n}_0U_1+\hat{v}_0N_1)'=0$ and $(\hat{v}_0U_1)'=0$. From the conditions $N_1(0)=U_1(0)=0$, we obtain $\hat{n}_0U_1+\hat{v}_0N_1=0$ and $\hat{v}_0U_1=0$ for all ζ, which yields $N_1(\zeta)=U_1(\zeta)=0$. The integration constants $N_2(\zeta)$ and $U_2(\zeta)$ are also determined by similar conditions for the secular terms of the third-order equations. After a straightforward calculation, we obtain $U_2=-\phi_1'^2/4v_0$ and $N_2=n_0\phi_1'^2/4v_0^2$.

We have thus derived the ion density and velocity profile in an rf sheath up to order ε^2 as

$$\hat{n}(\zeta,\tau)=\hat{n}_0(\zeta)+\varepsilon^2[-(\hat{n}_0\phi_1')'\cos\tau+(\hat{n}_0\phi_1'^2/4\hat{v}_0^2)], \tag{23}$$

$$\hat{v}(\zeta,\tau)=\hat{v}_0-\varepsilon\phi_1'\sin\tau-\varepsilon^2[(\hat{v}_0\phi_1')'\cos\tau+(\phi_1'^2/4\hat{v}_0)]. \tag{24}$$

By averaging Eqs. (23) and (24) over an rf cycle and dimensionalizing the resulting expressions, we obtain

$$\bar{n}=n_0\left(1+\frac{q^2E_1^2}{4m^2\omega^2v_{z0}^2}\right)=n_0\left[1+\frac{1}{2}\left(\frac{\omega_{pi}}{\omega}\right)^2\frac{\epsilon_0E_1^2/4}{\frac{1}{2}mn_0v_{z0}^2}\right], \tag{25}$$

$$\bar{v}=v_{z0}\left(1-\frac{q^2E_1^2}{4m^2\omega^2v_{z0}^2}\right)=v_{z0}\left[1-\frac{1}{2}\left(\frac{\omega_{pi}}{\omega}\right)^2\frac{\epsilon_0E_1^2/4}{\frac{1}{2}mn_0v_{z0}^2}\right], \tag{26}$$

where $n_0=n_I\hat{n}_0$, $v_{z0}=\varepsilon d\omega\hat{v}_0$, and $\omega_{pi}(z)=q\sqrt{n_0(z)/m\epsilon_0}$ denotes the local ion plasma frequency.

The steady-state momentum-conservation equation for the time-averaged velocity $\bar{v}_z$ is then derived from Eqs. (25) and (26), up to order ε^2, as follows:

$$m\bar{n}\bar{v}_z\frac{d\bar{v}_z}{dz}=-q\bar{n}\frac{d\Phi_0}{dz}-\left(\frac{\omega_{pi}}{\omega}\right)^2\frac{d}{dz}\left(\frac{\epsilon_0E_1^2(z)}{4}\right), \tag{27}$$

where Eq. (16) is used. The last term of Eq. (27) represents a force proportional to the time-averaged pressure (or energy density) of the oscillating field $E_1\cos\omega t$, which is known as the ponderomotive force or Miller's force.[11] Equation (27) describes ion fluid motion in the effective potential

$$\Phi_{\text{eff}}=\Phi_0(z)+\frac{qE_1^2(z)}{4m\omega^2}=\Phi_0(z)+\frac{1}{qn_0}\left(\frac{\omega_{pi}}{\omega}\right)^2\frac{\epsilon_0 E_1^2(z)}{4}. \tag{28}$$

A dynamical equation for single-particle motion in the ponderomotive-force potential is derived in Ref. 1.

Since the sheath electric field is generally an increasing function of z, the sense of the ponderomotive force is opposite to that of the dc field E_0, i.e., it retards the ion motion through the sheath from the plasma bulk to the cathode. Due to this retarding effect, as indicated in Eq. (26), the time-averaged ion kinetic energy is lower by $q^2E_1^2/4m\omega^2[\simeq(\omega_{\text{tr}}/\omega)^2\Phi_0$ when $E_1\simeq E_0\simeq\Phi_0/d]$ in rf sheaths than that in the corresponding dc sheath whose electric field is given by the dc-bias field $E_0(z)$. Consequently, the time-averaged ion density is higher in rf sheaths, since the time-averaged total flux nv_z is constant in space, as indicated in Eq. (25).

V. SUMMARY

In summary, we have discussed the transport of ions across collisionless rf sheaths. In the high-frequency regime, the "ponderomotive force" in a sheath field of oscillating magnitude was shown to exert a retarding effect on ions, causing the time-averaged ion flow velocity to be lower, and the number density higher, than in an equivalent dc sheath. We also considered sheaths in which the extent, rather than magnitude, of the field varies sinusoidally with time. In this model, the manner in which ions alternately accelerate and coast as they enter and leave the sheath field induces a sensitive dependence of the precise form of the ion energy distribution on the radio frequency. The ion energetics of real rf sheaths are expected to lie within the range of behavior observed in the idealized models described herein.

[1] S. Hamaguchi, R. T. Farouki, and M. Dalvie, Phys. Rev. Lett. **68**, 44 (1992).
[2] R. T. Farouki, S. Hamaguchi, and M. Dalvie, Phys. Rev. A **45**, 5913 (1992).
[3] R. T. Farouki, S. Hamaguchi, and M. Dalvie, Phys. Rev. A **44**, 2264 (1991).
[4] S. Hamaguchi, R. T. Farouki, and M. Dalvie, Phys. Rev. A **44**, 3804 (1991).
[5] J. W. Coburn and E. Kay, J. Appl. Phys. **43**, 4965 (1972).
[6] W. M. Holber and J. Forster, J. Vac. Sci. Technol. A **8**, 3720 (1990).
[7] M. J. Kushner, J. Appl. Phys. **58**, 4024 (1985).
[8] M. S. Barnes, J. C. Forster, and J. H. Keller, IEEE Trans. Plasma Sci. **PS-19**, 240 (1991).
[9] D. Bohm, in *The Characteristics of Electrical Discharges in Magnetic Fields*, edited by A. Guthrie and R. K. Wakerling (McGraw-Hill, New York, 1949), Chap. 3.
[10] P. Benoit-Cattin and L. C. Bernard, J. Appl. Phys. **39**, 5723 (1968).
[11] F. Chen, *Introduction to Plasma Physics* (Plenum, New York, 1974).